Science
AAAS

Coherent Control of a Single Electron Spin with Electric Fields
K. C. Nowack, *et al.*
Science **318**, 1430 (2007);
DOI: 10.1126/science.1148092

Science (print ISSN 0036-8075; online ISSN 1095-9203) is published weekly, except the last week in December, by the American Association for the Advancement of Science, 1200 New York Avenue NW, Washington, DC 20005.

ticles will depend on size due to quantum confinement effects.

References and Notes

1. M. I. Landstrass, K. V. Ravi, *Appl. Phys. Lett.* **55**, 975 (1989).
2. R. S. Gi *et al.*, *Jap. J. Appl. Phys. Part 1* **38**, 3492 (1999).
3. K. Hayashi, S. Yamanaka, H. Okushi, K. Kajimura, *Appl. Phys. Lett.* **68**, 376 (1996).
4. H. J. Looi *et al.*, *Diamond Relat. Mater.* **7**, 550 (1998).
5. R. S. Gi *et al.*, *Jap. J. Appl. Phys. Part 1* **36**, 2057 (1997).
6. A. Denisenko, A. Aleksov, E. Kohn, *Diamond Relat. Mater.* **10**, 667 (2001).
7. H. Kawarada, Y. Araki, T. Sakai, T. Ogawa, H. Umezawa, *Phys. Status Solidi* **185**, 79 (2001).
8. K. Hayashi *et al.*, *J. Appl. Phys.* **81**, 744 (1997).
9. T. Maki *et al.*, *Jap. J. Appl. Phys.* **31**, L1446 (1992).
10. F. Maier, M. Riedel, J. Mantel, J. Ristein, L. Ley, *Phys. Rev. Lett.* **85**, 3472 (2000).
11. J. Ristein, M. Riedel, L. Ley, *J. Electrochem. Soc.* **151**, E315 (2004).
12. K. Larsson, J. Ristein, *J. Phys. Chem. B* **109**, 10304 (2005).
13. D. Petrini, K. Larsson, *J. Phys. Chem. C* **111**, 13804 (2007).
14. J. Ristein, *Science* **313**, 1057 (2006).
15. D. Qi *et al.*, *J. Am. Chem. Soc.* **129**, 8084 (2007).
16. A. W. Adamson, *Physical Chemistry of Surfaces* (Wiley, New York, 1982).
17. J. S. Foord *et al.*, *Diamond Relat. Mater.* **11**, 856 (2002).
18. V. Chakrapani, S. C. Eaton, A. B. Anderson, M. Tabib-Azar, J. C. Angus, *Electrochem. Solid-State Lett.* **8**, E4 (2005).
19. A. J. Bard, R. Memming, B. Miller, *Pure Appl. Chem.* **63**, 569 (1991).
20. Yu. Ya. Gurevich, Yu. V. Pleskov, *Elektrokhimiya* **18**, 1477 (1982).
21. *C. R. C. Handbook of Chemistry and Physics*, D. R. Lide, Ed. (CRC Press, Boca Raton, FL, ed. 84, 2003).
22. Yu. V. Pleskov, A. Ya. Sakharova, M. D. Krotova, L. L. Bouilov, B. V. Spitsyn, *J. Electroanal. Chem.* **228**, 19 (1987).
23. G. Piantanida *et al.*, *J. Appl. Phys.* **89**, 8259 (2001).
24. F. Maier, J. Ristein, L. Ley, *Phys. Rev. B* **64**, 165411 (2001).
25. T. N. Rao, D. A. Tryk, K. Hashimoto, A. Fujishima, *J. Electrochem. Soc.* **146**, 680 (1999).
26. J. A. Dean, *Lange's Handbook of Chemistry* (McGraw-Hill, New York, ed. 15, 1999).
27. B. Rezek *et al.*, *Appl. Phys. Lett.* **82**, 2266 (2003).
28. P. C. Hiemenz, R. Rajagopalan, *Principles of Colloid and Surface Chemistry* (Dekker, New York, ed. 3, 1997).
29. A. W. Neumann, R. J. Good, *Techniques of Measuring Contact Angles, Surface and Colloid Science*, vol. II, *Experimental Methods*, R. J. Good, R. R. Stromberg, Eds. (Plenum, New York, 1979).
30. N. Matsuka, Y. Nakagawa, M. Kurihara, T. Tonomura, *Desalination* **51**, 163 (1984).
31. G. S. Woods, in *Properties and Growth of Diamond*, G. Davies, Ed. (EMIS Datareviews Ser. 9, Institution of Chemical Engineers, London, 1994), pp. 83–84.
32. T. Evans, in *The Properties of Natural and Synthetic Diamond*, J .E. Field, Ed. (Academic Press, London, 1992), p. 239.
33. A. T. Collins, E. C. Lightowlers, in *Properties of Diamond*, J. E. Field, Ed. (Academic Press, London, 1979), p. 99.
34. J. Ristein, M. Reidel, M. Stammler, B. F. Mantel, L. Ley, *Diamond Relat. Mater.* **11**, 350 (2002).
35. S. Kazaoui, N. Minami, N. Matsuda, H. Kataura, Y. Achiba, *Appl. Phys. Lett.* **78**, 3433 (2001).
36. J. Zhao, J. Han, J. Lu, *Phys. Rev. B* **65**, 1934011 (2002).
37. D. Lovall, M. Buss, E. Graugnard, R. P. Andres, R. Reifenberger, *Phys. Rev. B* **61**, 5683 (2000).
38. K. Bradley *et al.*, *Phys. Rev. Lett.* **85**, 4361 (2000).
39. G. U. Sumanasekera, C. K. W. Adu, S. Fang, P. C. Eklund, *Phys. Rev. Lett.* **85**, 1096 (2000).
40. P. G. Collins, K. Bradley, M. Ishigami, A. Zettl, *Science* **287**, 1801 (2000).
41. J. Kong *et al.*, *Science* **287**, 622 (2000).
42. S. Picozzi *et al.*, *J. Vac. Sci. Technol. A* **22**, 1466 (2004).
43. A. Zahab, L. Spina, P. Poncharal, C. Marlieri, *Phys. Rev. B* **62**, 10000 (2000).
44. K. M. Tracy, P. J. Hartlieb, R. F. Davis, E. H. Hurt, R. J. Nemanich, *J. Appl. Phys.* **94**, 3939 (2003).
45. V. M. Bermudez, *J. Appl. Phys.* **80**, 1190 (1996).
46. V. Chakrapani, thesis, Case Western Reserve University, Cleveland, OH (2007).
47. V. Chakrapani, J. C. Angus, A. B. Anderson, G. Sumanasekera, *Mater. Res. Soc. Symp. Proc.* **956,** paper 0956-J15-01 (2007)
48. J. A. Wiles, M. Fialkowski, M. R. Radowski, G. M. Whitesides, B. A. Grzybowski, *J. Phys. Chem. B* **108**, 20296 (2004).
49. S. Trigwell, N. Grable, C. U. Yurteri, R. Sharma, M. K. Mazumder, *IEEE Trans. Ind. Appl.* **39**, 79 (2003).

50. We thank J. Adin Mann and D. J. Lacks for useful discussions. C. C. Hayman provided invaluable experimental support. Financial support of the NSF (grant CHEM 0314688) and Case Western Reserve University is gratefully acknowledged.

6 August 2007; accepted 16 October 2007
10.1126/science.1148841

REPORTS

Coherent Control of a Single Electron Spin with Electric Fields

K. C. Nowack,*† F. H. L. Koppens,† Yu. V. Nazarov, L. M. K. Vandersypen*

Manipulation of single spins is essential for spin-based quantum information processing. Electrical control instead of magnetic control is particularly appealing for this purpose, because electric fields are easy to generate locally on-chip. We experimentally realized coherent control of a single-electron spin in a quantum dot using an oscillating electric field generated by a local gate. The electric field induced coherent transitions (Rabi oscillations) between spin-up and spin-down with 90° rotations as fast as ~55 nanoseconds. Our analysis indicated that the electrically induced spin transitions were mediated by the spin-orbit interaction. Taken together with the recently demonstrated coherent exchange of two neighboring spins, our results establish the feasibility of fully electrical manipulation of spin qubits.

Spintronics and spin-based quantum information processing provide the possibility of adding new functionality to today's electronic devices by using the electron spin in addition to the electric charge (*1*). In this context, a key element is the ability to induce transitions between the spin-up and spin-down states of a localized electron spin and to prepare arbitrary superpositions of these two basis states. This is commonly accomplished by magnetic resonance, whereby bursts of a resonant oscillating magnetic field are applied (*2*). However, producing strong oscillating magnetic fields in a semiconductor device requires specially designed microwave cavities (*3*) or microfabricated striplines (*4*), and this has proven to be challenging. In comparison, electric fields can be generated much more easily, simply by exciting a local gate electrode. In addition, this allows for greater spatial selectivity, which is important for local addressing of individual spins. It would thus be highly desirable to control the spin by means of electric fields.

Although electric fields do not couple directly to the electron spin, indirect coupling can still be realized by placing the spin in a magnetic field gradient (*5*) or in a structure with a spatially varying g tensor, or simply through spin-orbit interaction, present in most semiconductor structures (*6*, *7*). Several of these mechanisms have been used to electrically manipulate electron spins in two-dimensional electron systems (*8*–*11*), but proposals for coherent electrical control at the level of a single spin (*5*, *12*–*15*) have so far remained unrealized.

We demonstrate coherent single spin rotations induced by an oscillating electric field. The electron is confined in a gate-defined quantum dot (Fig. 1A), and we use an adjacent quantum dot, containing one electron as well, for readout. The ac electric field is generated through excitation of one of the gates that form the dot, thereby

Kavli Institute of Nanoscience, Delft University of Technology, Post Office Box 5046, 2600 GA Delft, the Netherlands.

*To whom correspondence should be addressed. E-mail: k.c.nowack@tudelft.nl, l.m.k.vandersypen@tudelft.nl
†These authors contributed equally to this work.

periodically displacing the electron wave function around its equilibrium position (Fig. 1B).

The experiment consists of four stages (Fig. 1C). The device is initialized in a spin-blockade regime where two excess electrons, one in each dot, are held fixed with parallel spins (spin triplet), either pointing along or opposed to the external magnetic field [the system is never blocked in the triplet state with antiparallel spins, because of the effect of the nuclear fields in the two dots combined with the small interdot tunnel coupling; see (*16*) for details]. Next, the two spins are isolated by a gate voltage pulse, such that electron tunneling between the dots or to the reservoirs is forbidden. Then, one of the spins is rotated by an ac voltage burst applied to the gate, over an angle that depends on the length of the burst (*17*) (most likely the spin in the right dot, where the electric field is expected to be strongest). Finally, the readout stage allows the left electron to tunnel to the right dot if and only if the spins are antiparallel. Subsequent tunneling of one electron to the right reservoir gives a contribution to the current. This cycle is repeated continuously, and the current flow through the device is thus proportional to the probability of having antiparallel spins after excitation.

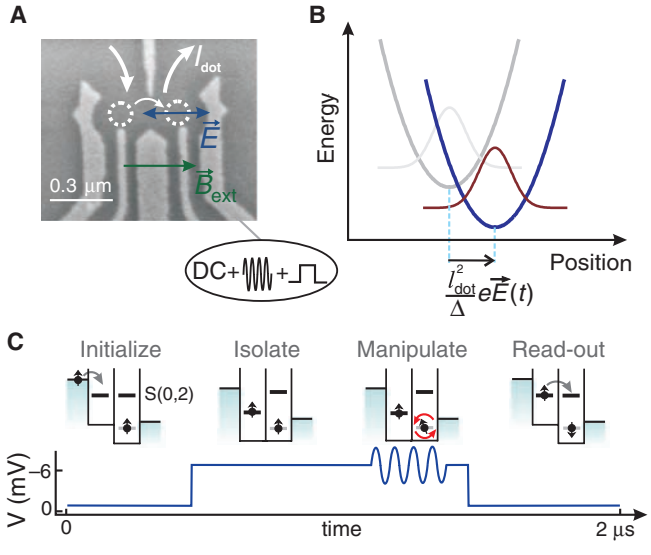

Fig. 1. (**A**) Scanning electron micrograph of a device with the same gate structure as the one used in this experiment. Metallic TiAu gates are deposited on top of a GaAs heterostructure that hosts a two-dimensional electron gas 90 nm below the surface. Not shown is a coplanar stripline on top of the metallic gates, separated by a dielectric [not used in this experiment; see also (*4*)]. In addition to a dc voltage, we can apply fast pulses and microwaves to the right side gate (as indicated) through a homemade bias-tee. The orientation of the in-plane external magnetic field is as shown. (**B**) The electric field generated upon excitation of the gate displaces the center of the electron wave function along the electric field direction and changes the potential depth. Here, Δ is the orbital energy splitting, $l_{dot} = \hbar/\sqrt{m^*\Delta}$ the size of the dot, m^* the effective electron mass, $\hbar$ the reduced Planck constant, and $\mathbf{E}(t)$ the electric field. (**C**) Schematic of the spin manipulation and detection scheme, controlled by a combination of a voltage pulse and burst, $V(t)$, applied to the right side gate. The diagrams show the double dot, with the thick black lines indicating the energy cost for adding an extra electron to the left or right dot, starting from (0,1), where (n,m) denotes the charge state with n and m electrons in the left and right dot. The energy cost for reaching (1,1) is (nearly) independent of the spin configuration. However, for (0,2), the energy cost for forming a singlet state [indicated by $S(0,2)$] is much lower than that for forming a triplet state (not shown). This difference is exploited for initialization and detection, as explained further in the main text.

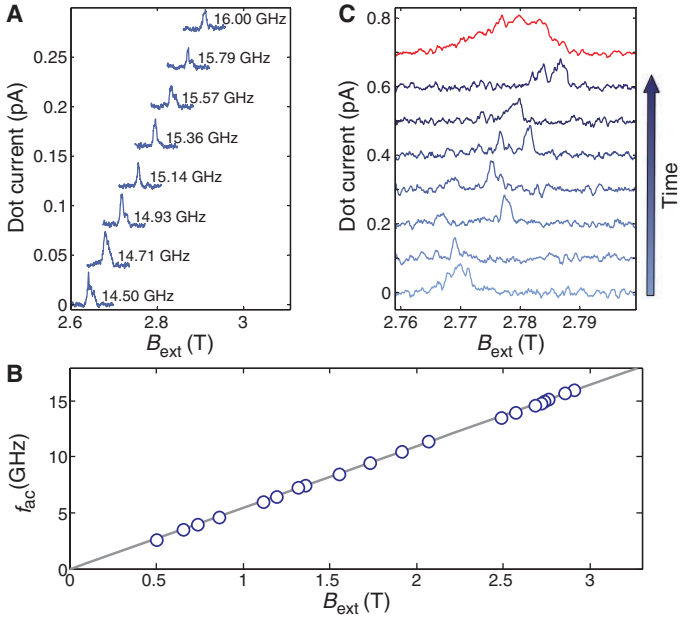

Fig. 2. (**A**) The current averaged over 40 magnetic field sweeps is given for eight different excitation frequencies, with a microwave burst length of 150 ns. The traces are offset for clarity. The microwave amplitude V_{mw} was in the range 0.9 to 2.2 mV, depending on the frequency (estimated from the output power of the microwave source and taking into account the attenuation of the coaxial lines and the switching circuit used to create microwave bursts). (**B**) Position of the resonant response over wider frequency and field ranges. Error bars are smaller than the size of the circles. (**C**) Individual magnetic field sweeps at f_{ac} = 15.2 GHz measured by sweeping from high to low magnetic field with a rate of 50 mT/min. The traces are offset by 0.1 pA each for clarity. The red trace is an average over 40 sweeps, including the ones shown and scaled up by a factor of 5.

In addition to the external magnetic field, the electron spin feels an effective nuclear field B_N arising from the hyperfine interaction with nuclear spins in the host material and fluctuating in time (*19*, *20*). This nuclear field modifies the electron spin resonance condition and is generally different in the left and right dot (by ΔB_N). The peaks shown in Fig. 2A are averaged over many magnetic field sweeps and have a width of about 10 to 25 mT. This is much larger than the expected linewidth, which is only 1 to 2 mT as given by the statistical fluctuations of B_N (*21*, *22*). Looking at individual field sweeps measured at constant excitation frequency, we see that the peaks are indeed a few mT wide (Fig. 2C), but that the peak positions change in time over a range of ~20 mT. Judging from the dependence of the position and shape of the averaged peaks on sweep direction, the origin of this large variation in the nuclear field is most likely dynamic nuclear polarization (*4*, *23*–*26*).

To demonstrate coherent control of the spin, we varied the length of the microwave bursts and monitored the current level. In Fig. 3A we plot the maximum current per magnetic field sweep as a function of the microwave burst duration, averaged over several sweeps (this is a more sensitive method than averaging the traces first and then taking the maximum) (*17*). The maximum current exhibits clear oscillations as a function of burst length. Fitting with a cosine function reveals a linear scaling of the oscilla-

tion frequency with the driving amplitude (Fig. 3B), a characteristic feature of Rabi oscillations and proof of coherent control of the electron spin via electric fields.

The highest Rabi frequency we achieved is ~4.7 MHz (measured at f_{ac} = 15.2 GHz), corresponding to a 90° rotation in ~55 ns, which is only a factor of 2 slower than those realized with magnetic driving (*4*). Stronger electrical driving was not possible because of photon-assisted tunneling. This is a process whereby the electric field provides energy for one of the following transitions: tunneling of an electron to a reservoir or to the triplet with both electrons in the right dot. This lifts spin blockade, irrespective of whether the spin resonance condition is met.

Small Rabi frequencies could be observed as well. The bottom trace of Fig. 3A shows a Rabi oscillation with a period exceeding 1.5 μs (measured at f_{ac} = 2.6 GHz), corresponding to an effective driving field of only about 0.2 mT, one-tenth the amplitude of the statistical fluctuations of the nuclear field. The oscillations are nevertheless visible because the dynamics of the nuclear bath are slow compared to the Rabi period, resulting in a slow power-law decay of the oscillation amplitude on driving field (*27*).

We next turn to the mechanism responsible for resonant transitions between spin states. First, we exclude a magnetic origin because the oscillating magnetic field generated upon excitation of the gate is more than two orders of magnitude too small to produce the observed Rabi oscillations with periods up to ~220 ns, which requires a driving field of about 2 mT (*17*). Second, we have seen that there are in principle a number of ways in which an ac electric field can cause single-spin transitions. What is required is that the oscillating electric field give rise to an effective magnetic field, $\mathbf{B}_{eff}(t)$, acting on the spin, oscillating in the plane perpendicular to $\mathbf{B}_{ext}$, at frequency $f_{ac} = g\mu_B|\mathbf{B}_{ext}|/h$. The g-tensor anisotropy is very small in GaAs, so g-tensor modulation can be ruled out as the driving mechanism. Furthermore, in our experiment there is no external magnetic field gradient applied, which could otherwise lead to spin resonance (*5*). We are aware of only two remaining possible coupling mechanisms: spin-orbit interaction and the spatial variation of the nuclear field.

In principle, moving the wave function in a nuclear field gradient can drive spin transitions (*5*, *28*), as was recently observed (*26*). However, the measurement of each Rabi oscillation lasted more than 1 hour, much longer than the time during which the nuclear field gradient is constant (~100 μs to a few s). Because this field gradient and, therefore, the corresponding effective driving field, slowly fluctuates in time around zero, the oscillations would be strongly damped, regardless of the driving amplitude (*26*). Possibly, a (nearly) static gradient in the nuclear spin polarization could develop as a result of electron-nuclear feedback. However, such polarization would be parallel to $\mathbf{B}_{ext}$ and thus cannot be responsible for the observed coherent oscillations.

In contrast, spin orbit–mediated driving can induce coherent transitions (*12*), which can be understood as follows. The spin-orbit interaction in a GaAs heterostructure is given by $H_{SO} = \alpha(p_x\sigma_y - p_y\sigma_x) + \beta(-p_x\sigma_x + p_y\sigma_y)$, where α and β are the Rashba and Dresselhaus spin-orbit coefficient, respectively, and $p_{x,y}$ and $\sigma_{x,y}$ are the momentum and spin operators in the x and y directions (along the [100] and [010] crystal directions, respectively). As suggested in (*13*), the spin-orbit interaction can be conveniently accounted for up to the first order in α, β by applying a (gauge) transformation, resulting in a position-dependent correction to the external magnetic field. This effective magnetic field, acting on the spin, is proportional and orthogonal to the field applied

$$\mathbf{B}_{eff}(x,y) = \mathbf{n}\otimes\mathbf{B}_{ext};\ n_x = \frac{2m^*}{\hbar}(-\alpha y - \beta x);\quad n_y = \frac{2m^*}{\hbar}(\alpha x + \beta y);\ n_z = 0 \qquad (1)$$

An electric field $\mathbf{E}(t)$ will periodically and adiabatically displace the electron wave function (Fig. 1B) by $\mathbf{x}(t) = (el_{dot}^2/\Delta)\mathbf{E}(t)$, so the electron spin will feel an oscillating effective field $\mathbf{B}_{eff}(t) \perp \mathbf{B}_{ext}$ through the dependence of $\mathbf{B}_{eff}$ on the position. The direction of $\mathbf{n}$ can be constructed from the direction of the electric field as shown in Fig. 4C and together with the direction of $\mathbf{B}_{ext}$ determines how effectively the electric field couples to the spin. The Rashba contribution always gives $\mathbf{n}\perp\mathbf{E}$, while for the Dresselhaus contribution this depends on the orientation of the electric field with respect to the crystal axis. Given the gate geometry, we expect the dominant electric field to be along the double dot axis (Fig. 1A), which here is either the [110] or [1$\bar{1}$0] crystallographic direction. For these orientations, the Dresselhaus contribution is also orthogonal to the electric field (Fig. 4C). This is why both contributions will give $\mathbf{B}_{eff} \neq 0$ and lead to coherent oscillations in the present experimental geometry, where $\mathbf{E} \parallel \mathbf{B}_{ext}$. In (*26*), a very similar gate geometry was used, but the orientation of $\mathbf{B}_{ext}$ was different, and it

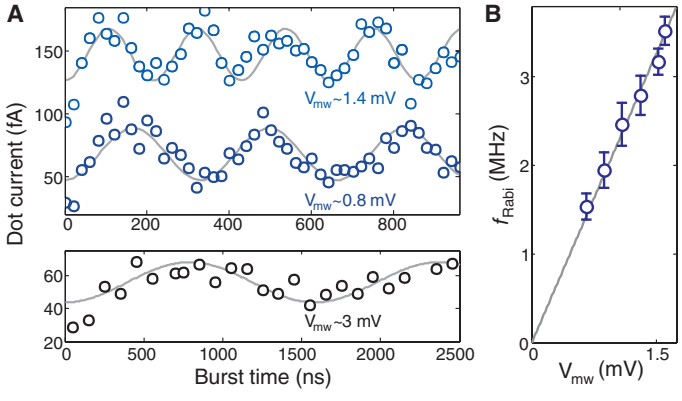

Fig. 3. (**A**) Rabi oscillations at 15.2 GHz (blue, average over five sweeps) and 2.6 GHz (black, average over six sweeps). The two oscillations at 15.2 GHz are measured at different amplitudes of the microwaves V_{mw}, leading to different Rabi frequencies. (**B**) Linear dependence of the Rabi frequency on applied microwave amplitude measured at f_{ac} = 14 GHz.

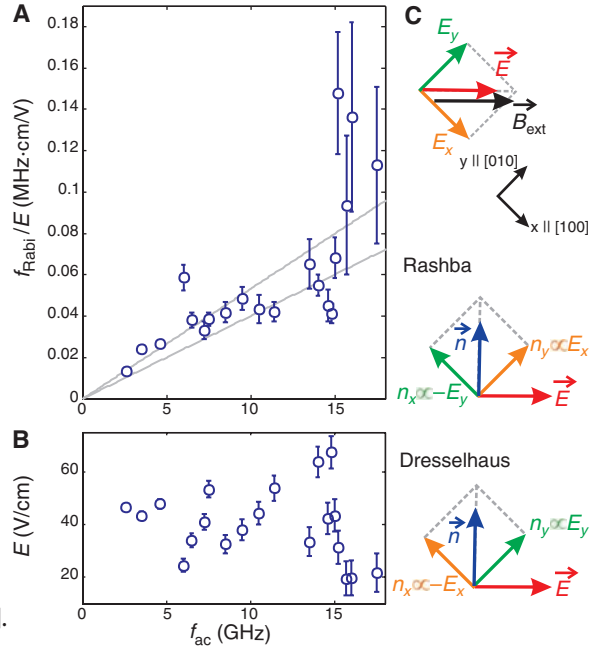

Fig. 4. (**A**) Rabi frequency rescaled with the applied electric field for different excitation frequencies. The error bars are given by

$$f_{Rabi}/E \cdot\sqrt{(\delta E/E)^2 + (\delta f_{Rabi}/f_{Rabi})^2}$$

where δf_{Rabi} and δE are the error in the Rabi frequency and electric field amplitude, respectively. The gray lines are the 95% confidence bounds for a linear fit through the data (weighting the data points by the inverse error squared). (**B**) Estimated electric field amplitudes at which the Rabi oscillations of (A) were measured at the respective excitation frequencies (*17*). (**C**) Construction of the direction of $\mathbf{n}$ resulting from the Rashba and Dresselhaus spin-orbit interaction for an electric field along [110] following Eq. 1. The coordinate system is set to the crystallographic axis [100] and [010].

can be expected that $\mathbf{E} \perp \mathbf{B}_{ext}$. In that experiment, no coherent oscillations were observed, which is consistent with the considerations here.

An important characteristic of spin orbit–mediated driving is the linear dependence of the effective driving field on the external magnetic field, which follows from Eq. 1 and is predicted in (*12*, *13*, *29*). We aim to verify this dependence by measuring the Rabi frequency as a function of the resonant excitation frequency (Fig. 4A), which is proportional to the external magnetic field. Each point is rescaled by the estimated applied electric field (Fig. 4B). Even at fixed output power of the microwave source, the electric field at the dot depends on the microwave frequency due to various resonances in the line between the microwave source and the gate (caused by reflections at the bonding wires and microwave components). However, we use the photon-assisted–tunneling response as a probe for the ac voltage drop across the interdot tunnel barrier, which we convert into an electric field amplitude by assuming a typical interdot distance of 100 nm. This allows us to roughly estimate the electric field at the dot for each frequency (*17*). Despite the large error bars, which predominantly result from the error made in estimating the electric field, an overall upward trend is visible in Fig. 4A.

For a quantitative comparison with theory, we extract the spin-orbit strength in GaAs, via the expression of the effective field $\mathbf{B}_{eff}$ perpendicular to $\mathbf{B}_{ext}$ for the geometry of this experiment (*12*)

$$|\mathbf{B}_{eff}(t)| = 2\,|\mathbf{B}_{ext}|\,\frac{l_{dot}}{l_{SO}}\,\frac{e|\mathbf{E}(t)|l_{dot}}{\Delta} \qquad (2)$$

with l_{SO} the spin-orbit length (for the other definitions, see Fig. 1B). Here, $l_{SO}^{-1} = m^*(\alpha \mp \beta)/\hbar$ for the case with the gate symmetry axis along $[1\bar{1}0]$ or [110], respectively. Via $f_{Rabi} = (g\mu_B|\mathbf{B}_{eff}|)/2h$, the confidence interval of the slope in Fig. 4A gives a spin-orbit length of 28 to 37 μm (with a level splitting Δ in the right dot of 0.9 meV extracted from high-bias transport measurements). Additional uncertainty in l_{SO} is due to the estimate of the interdot distance and the assumption of a homogeneous electric field, deformation effects of the dot potential (*15*), and extra cubic terms in the Hamiltonian (*7*). Still, the extracted spin-orbit length is of the same order of magnitude as other reported values for GaAs quantum dots (*18*).

Both the observed trend of $\mathbf{B}_{eff}$ with f_{ac} and the extracted range for l_{SO} are consistent with our supposition (by elimination of other mechanisms) that spin transitions are mediated by spin-orbit interaction. We note that also for relaxation of single electron spins in which electric field fluctuations from phonons couple to the spin, it is by now well established that the spin-orbit interaction is dominant at fields higher than a few 100 mT (*12*, *18*, *28*, *29*). It can thus be expected to be dominant for coherent driving as well.

The electrically driven single-spin resonance reported here, combined with the so-called $\sqrt{SWAP}$ gate based on the exchange interaction between two neighboring spins (*30*), brings all-electrical universal control of electron spins within reach. Whereas the $\sqrt{SWAP}$ gate already operates on subnanosecond time scales, single-spin rotations still take about 100 ns (the main limitation is photon-assisted tunneling). Faster operations could be achieved by suppressing photon-assisted tunneling (e.g., by increasing the tunnel barriers or operating deeper into Coulomb blockade), by working at still higher magnetic fields, by using materials with stronger spin-orbit interaction, or through optimized gate designs. Furthermore, the electrical control offers the potential for spatially selective addressing of individual spins in a quantum dot array, because the electric field is produced by a local gate. Finally, the spin rotations were realized at magnetic fields high enough to allow for single-shot read-out of a single spin (*31*), so that both elements can be integrated in a single experiment.

References and Notes

1. D. Awschalom, D. Loss, N. Samarth, *Semiconductor Spintronics and Quantum Computation* (Springer-Verlag, Berlin, 2002).
2. C. Poole, *Electron Spin Resonance* (Wiley, New York, ed. 2, 1983).
3. B. Simovič *et al.*, *Rev. Sci. Instrum.* **77**, 064702 (2006).
4. F. H. L. Koppens *et al.*, *Nature* **442**, 766 (2006).
5. Y. Tokura, W. G. Van der Wiel, T. Obata, S. Tarucha, *Phys. Rev. Lett.* **96**, 047202 (2006).
6. Y. A. Bychkov, E. I. Rashba, *J. Phys. C* **17**, 6039 (1984).
7. G. Dresselhaus, *Phys. Rev.* **100**, 580 (1955).
8. Y. Kato, R. C. Myers, A. C. Gossard, D. D. Awschalom, *Nature* **427**, 50 (2003).
9. Y. Kato *et al.*, *Science* **299**, 1201 (2003).
10. G. Salis *et al.*, *Nature* **414**, 619 (2001).
11. M. Schulte, J. G. S. Lok, G. Denninger, W. Dietsche, *Phys. Rev. Lett.* **94**, 137601 (2005).
12. V. N. Golovach, M. Borhani, D. Loss, *Phys. Rev. B* **74**, 165319 (2006).
13. L. Levitov, E. Rashba, *Phys. Rev. B* **67**, 115324 (2003).
14. S. Debald, C. Emary, *Phys. Rev. Lett.* **94**, 226803 (2005).
15. J. Walls, *Condens. Matter*, http://arxiv.org/abs/0705.4231 (2007).
16. F. H. L. Koppens *et al.*, *J. Appl. Phys.* **101**, 081706 (2007).
17. Supporting material is available on *Science* Online.
18. R. Hanson, L. P. Kouwenhoven, J. R. Petta, S. Tarucha, L. M. K. Vandersypen, *Rev. Mod. Phys.* **79**, 1217 (2007).
19. A. V. Khaetskii, D. Loss, L. Glazman, *Phys. Rev. Lett.* **88**, 186802 (2002).
20. I. A. Merkulov, A. L. Efros, M. Rosen, *Phys. Rev. B* **65**, 205309 (2002).
21. A. C. Johnson *et al.*, *Nature* **435**, 925 (2005).
22. F. H. L. Koppens *et al.*, *Science* **309**, 1346 (2005).
23. J. Baugh, Y. Kitamura, K. Ono, S. Tarucha, *Phys. Rev. Lett.* **99**, 096804 (2007).
24. M. S. Rudner, L. S. Levitov, *Phys. Rev. Lett.* **99**, 036602 (2007).
25. D. Klauser, W. A. Coish, D. Loss, *Phys. Rev. B* **73**, 205302 (2006).
26. E. A. Laird *et al.*, *Condens. Matter*, http://arxiv.org/abs/0707.0557 (2007).
27. F. H. L. Koppens *et al.*, *Phys. Rev. Lett.* **99**, 106803 (2007).
28. S. I. Erlingsson, Y. V. Nazarov, *Phys. Rev. B* **66**, 155327 (2002).
29. A. V. Khaetskii, Y. V. Nazarov, *Phys. Rev. B* **64**, 125316 (2001).
30. J. R. Petta *et al.*, *Science* **309**, 2180 (2005).
31. J. M. Elzerman *et al.*, *Nature* **430**, 431 (2004).

32. We thank L. P. Kouwenhoven, C. Barthel, E. Laird, M. Flatté, I. T. Vink, and T. Meunier for discussions and R. Schouten, B. van der Enden, and R. Roeleveld for technical assistance and J. H. Plantenberg and P. C. de Groot for help with microwave components. Supported by the Dutch Organization for Fundamental Research on Matter (FOM) and the Netherlands Organization for Scientific Research (NWO).

Supporting Online Material

www.sciencemag.org/cgi/content/full/1148092/DC1
Materials and Methods
SOM Text
Figs. S1 and S2
References

20 July 2007; accepted 16 October 2007
Published online 1 November 2007;
10.1126/science.1148092
Include this information when citing this paper.

Flow of Mantle Fluids Through the Ductile Lower Crust: Helium Isotope Trends

B. Mack Kennedy[1] and Matthijs C. van Soest[2]

Heat and mass are injected into the shallow crust when mantle fluids are able to flow through the ductile lower crust. Minimum $^3He/^4He$ ratios in surface fluids from the northern Basin and Range Province, western North America, increase systematically from low crustal values in the east to high mantle values in the west, a regional trend that correlates with the rates of active crustal deformation. The highest ratios occur where the extension and shear strain rates are greatest. The correspondence of helium isotope ratios and active transtensional deformation indicates a deformation-enhanced permeability and that mantle fluids can penetrate the ductile lithosphere, even in regions where there is no substantial magmatism. Superimposed on the regional trend are local, high $^3He/^4He$ anomalies indicating hidden magmatic activity and/or deep fluid production with locally enhanced permeability, identifying zones with high resource potential, particularly for geothermal energy development.

Mantle volatiles, principally water and CO_2, play an important role in lithospheric rheology and the production of buoyant fluids that can be injected into the shallow crust. Regional and local trends in the crustal occurrence of mantle volatiles provide insight into the coupling between mantle-crust tectonics (*1*, *2*), heat and mass exchange between the mantle and crust (*3*–*5*), and the occurrence and distribution of economic resources